Applied Surface Science 424 (2017) 82–86

Contents lists available at ScienceDirect

Applied Surface Science

journal homepage: www.elsevier.com/locate/apsusc

Full Length Article

Bias polarization study of steam electrolysis by composite oxygen electrode $Ba_{0.5}Sr_{0.5}Co_{0.8}Fe_{0.2}O_{3-\delta}/BaCe_{0.4}Zr_{0.4}Y_{0.2}O_{3-\delta}$

Tao Yang[a,*], Aliaksandr Shaula[a], D. Pukazhselvan[a], Devaraj Ramasamy[a], Jiguang Deng[b], E.L. da Silva[c], Ricardo Duarte[d], Jorge A. Saraiva[d]

[a] TEMA-NRG, Mechanical Engineering Department, University of Aveiro, Portugal
[b] College of Environmental and Energy Engineering, Beijing University of Technology, Beijing, China
[c] Department of Chemistry, University of Bath, Bath, United Kingdom
[d] QOPNA, Chemistry Department, University of Aveiro, 3810-193 Aveiro, Portugal

ARTICLE INFO

Article history:
Received 30 September 2016
Received in revised form 7 February 2017
Accepted 10 February 2017
Available online 14 February 2017

Keywords:
Protonic conductor
Steam electrolysis
Bias polarization
Electrochemical impedance spectroscopy

ABSTRACT

The polarization behavior of $Ba_{0.5}Sr_{0.5}Co_{0.8}Fe_{0.2}O_{3-\delta}$-$BaCe_{0.4}Zr_{0.4}Y_{0.2}O_{3-\delta}$ (BSCF-BCZY) electrode under steam electrolysis conditions was studied in detail. The composite oxygen electrode supported by BCZY electrolyzer has been assessed as a function of temperature (T), water vapor partial pressures (pH_2O), and bias polarization voltage for electrodes of comparable microstructure. The Electrochemical impedance spectra show two depressed arcs in general without bias polarization. And the electrode resistance became smaller with the increase of the bias polarization under the same water vapor partial pressures. The total resistance of the electrode was shown to be significantly affected by temperature, with the same level of pH_2O and bias polarization voltage. This result highlights BSCF-BCZY as an effective oxygen electrode under moderate polarization and pH_2O conditions.

1. Introduction

Hydrogen is essential for many current industrial processes and is envisaged to become an even more important resource in the future, both for the chemical industry and also as a secondary energy carrier [1–4]. Thus, a distinct market opportunity is opening for novel electrically-efficient electrolysis for the commercial production of hydrogen. Although the utilization of waste heat can maximize the electrical efficiency in high temperature electrolysis, the concept has not been extensively studied and to date has largely focused on oxide-ion conducting devices operating in the temperature range 800–1000 °C [5–7]. At 600–700 °C, favored for materials stability and infrastructure costs, proton-conducting electrolyte materials offer advantages over the oxide-ion conducting electrolytes due to their higher ion conductivities at these temperatures [8–10]. Proton conducting electrolysers offer an additional benefit that completely dry H_2 can be formed in contrast to the "wet" H_2 formed when using an oxide-ion conducting electrolyte. Despite these advantages, the status of proton ceramic electrolyser cells is only at the formative stage. The invention of new catalysts and/or new processing methods for protonic ceramic fuel cells (PCECs) is, therefore, essential. An ideal anode must offer high catalytic activity for steam dissociation as well as providing low polarization resistance. Polarization losses typically arise due to slow reaction kinetics and/or poor gas phase diffusion. Inward steam gas transport must occur at the same time as oxygen counter-diffusion at this electrode. To enhance the counter diffusion of oxygen the inclusion of a suitable oxide-ion conducting phase may be beneficial, in addition to the electronic and proton conducting phases in the anode. Moreover, the oxide-ion conducting phase must offer sufficient oxide-ion conduction at the relatively low temperature of ~750 °C. This is especially important as electrode delamination is a limiting problem in ceramic electrolysers and arises due to poor oxygen transport at the electrode/electrolyte interface. As typical oxide-ion conductors, e.g. yttria stabilised zirconia, may not offer sufficient conduction at these temperatures, the use of less common oxide-ion conductors may be required. New anodes with the ability to conduct ion, proton, and electron must be designed that are catalytically active for the steam dissociation reaction, while, simultaneously, ensuring excellent electrochemical performance with low polarization losses. In this respect, oxide-ion and electronic conductors, such as $Ba_{0.5}Sr_{0.5}Co_{0.8}Fe_{0.2}O_{3-\delta}$ (BSCF) and protonic conductor such as $BaCe_{0.4}Zr_{0.4}Y_{0.2}O_{3-\delta}$ (BCZY) would be considered due to our former research [11,12]. The current work is to assess the polarization behavior of $Ba_{0.5}Sr_{0.5}Co_{0.8}Fe_{0.2}O_{3-\delta}$-$BaCe_{0.4}Zr_{0.4}Y_{0.2}O_{3-\delta}$ (BSCF-BCZY) electrode as a function of temperature (T), water vapor

* Corresponding author.
E-mail addresses: yangtao@ua.pt, 21825550@qq.com (T. Yang).

http://dx.doi.org/10.1016/j.apsusc.2017.02.080
0169-4332/

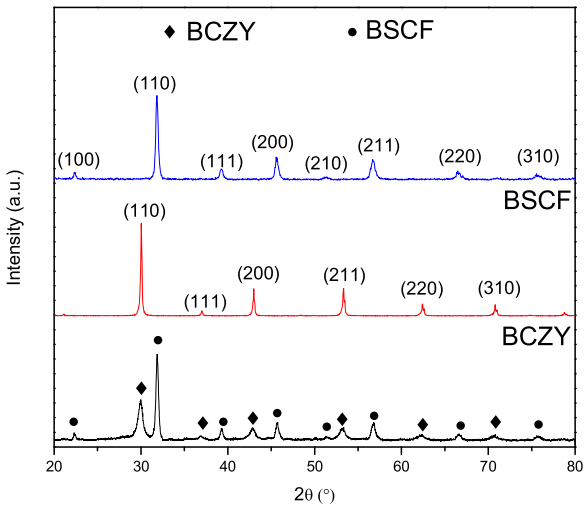

Fig. 1. X-ray powder diffraction patterns of BSCF, BCZY and the BSCF+BCZY electrode film after sintering.

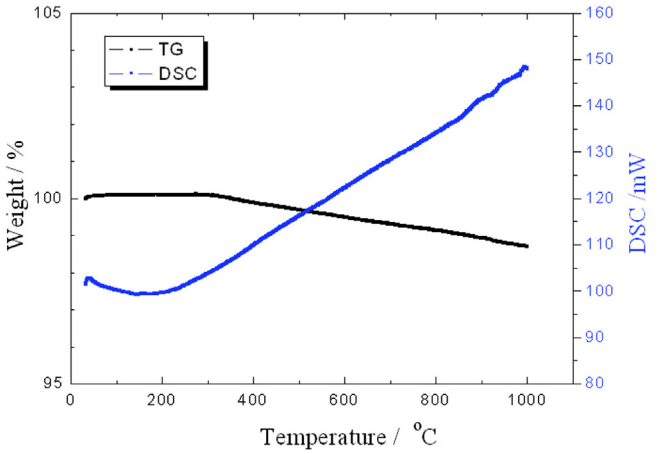

Fig. 2. TGA/DSC analysis of the BSCF+BCZY composite from room temperature to 1000 °C.

partial pressures (pH2O) in nitrogen, and bias polarization voltage for electrodes of comparable microstructure.

2. Experimental section

2.1. Synthesis of the samples

The ceramics studied in this work had the composition of $BaCe_{0.4}Zr_{0.4}Y_{0.2}O_{3-\delta}$ (BCZY) and was synthesized by an acetate-H_2O_2 combustion method developed by the group [13]. $Ba(CH_3COO)_2$ >99.9% pure, Sigma Aldrich), Zr(IV) $(CH_3COO)_x(OH)_y$ (99.9% pure, Sigma Aldrich), $Ce(CH_3COO)_3{\cdot}1.5H_2O$ (99.9% pure, Alfa Aesar), $Y(CH_3COO)_3{\cdot}4H_2O$ (99.9% pure, Alfa Aesar) and 30% H_2O_2 (Sigma Aldrich, 30% by weight) were used as starting materials for the combustion method. First, stoichiometric amounts of the metal acetates were dissolved in distilled water with constant stirring at 25 °C to obtain a clear, transparent solution. To the solution 30% H_2O_2 was added slowly to achieve a fuel to oxidant ratio of unity as per the propellant chemistry [14]. An orange-brown color solution with bubbles was observed and subsequently the solution was heated on a hot plate at 80 °C with constant stirring to form a viscous gel. Upon heating the orange-brown color transforms to a pale yellow. The viscous gel was then subjected to microwave heating, under rotation, in a domestic 2.45 GHz, 800 W microwave oven set at the maximum power. After a few minutes, the dried gel burnt with a flame in a self-propagating combustion manner, releasing plentiful fumes, to form a black powder. The combustion powder was fired at 1100 °C for 6 h in order to obtain the pure perovskite phase.

Powders of $Ba_{0.5}Sr_{0.5}Co_{0.8}Fe_{0.2}O_{3-\delta}$ were prepared using the Pechini method, starting from Sigma-Aldrich chemicals of $Ba(NO_3)_2$ (99.0%), $Sr(NO_3)_2$ (ACS reagent, ≥99.0%), $Fe(NO_3)_3{\cdot}9H_2O$ (99.99%), $Co(NO_3)_2{\cdot}6H_2O$ (ACS reagent, ≥99.0%) and citric acid (ACS reagent, ≥99.5%) (metal:acid ratio was 1:5). The formed gel was heated in air at 280 °C for 2 h and calcined further at 900 °C for 20 h.

After reaction, the aforementioned-synthesized BSCF and BCZY powders were ground in a mortar together and then ball-milled for 5 h at 450 rpm (PM200, Retsch, Haan, Germany).

2.2. Fabrication of the BCZY supported half cells

BCZY discs of 15 mm diameter and of 1.0 mm thickness were obtained by uniaxial pressing at 80 MPa for 30 s. Then, the discs were sealed in vacuum in plastic bags. A hydrostatic press (Hiperbaric 55, Hiperbaric, Burgos, Spain) was utilized to press the pellets in a pressures 350 MPa. This equipment has a pressure vessel of 200 mm inner diameter and 2000 mm length and a maximum operation pressure of 750 MPa. It is connected to a refrigeration unit (RMA KH 40 LT, Ferroli, San Bonifacio, Italy) that allows it to control the temperature of the input water used as a pressurizing fluid. All the hydrostatic press lasted 30 min. After press, the pellets were sintered at 1600 °C temperatures for 5 h to densify to 95%, with heating and cooling rates of 1.5 °C min^{-1}. BSCF and BCZY (40:60 vol%) particle suspensions were prepared by ball-mill at 400 rpm for 2 h followed by ultrasonic bath (Ultrasons-H, JPSELECTA, Abrera, Spain) for 1 h, to break agglomerates and reduce the particle size distribution. The thin electrode films (0.264 cm^2 of effective electroactive area) were deposited over the electrolyte support by spin coating (spin coater model WS-650-23, Laurell Technologies Corporation, North Wales PA, USA) at 2000 rpm for 30 s. The electrode-electrolyte assemblies were obtained by sintering in air at 1000 °C for 5 h, with heating and cooling rates of 1.5 °C min^{-1}. The diameter of the electrode was 5 mm. Porous Pt-paste was used as both counter and reference electrode. The distance between reference electrode in the edge and the working electrode is 20 times of the thickness of the electrolyte.

2.3. Characterization

The calcined powders and the sintered samples were analyzed by X-ray diffraction analysis (XRD) using a German Bruker D-8 Advance Diffractometer with Cu Kα (λ = 1.5405 Å) radiation with a scanning speed of 2° min^{-1} and a stepsize of 0.02°. A Jeol JSM-6500F scanning electron microscope (SEM) was used to observe the microstructure of the sintered ceramics, as well as an energy dispersive X-Ray spectrometer (EDS) to perform elemental mapping of the samples. The density of sintered pellets was calculated by their weight and geometry. Thermogravimetric (TGA) analysis and differential scanning calorimetry (DSC) were carried out using the Netzsch Jupiter instrument in dry air atmosphere with heating rates of 5 °C min^{-1}. Electrical-conductivity measurements were performed on the BSCF-BCZY/BCZY/Pt cell. Platinum wire was attached to the cell in a 3-point configuration using porous Pt-paste. Impedance spectroscopy was carried out using an Electrochemie Autolab PGSTAT302N analyser in the frequency range 10^{-2}–10^6 Hz, amplitude 50 mV. Bias polarization voltage was applied between the BSCF-BCZY/Pt electrodes. Data were collected on cooling in flowing of steam and N_2. The measurements were carried out using H_2O percentage of 0%, 3%, 10%, and 20% in 99.999% N_2.

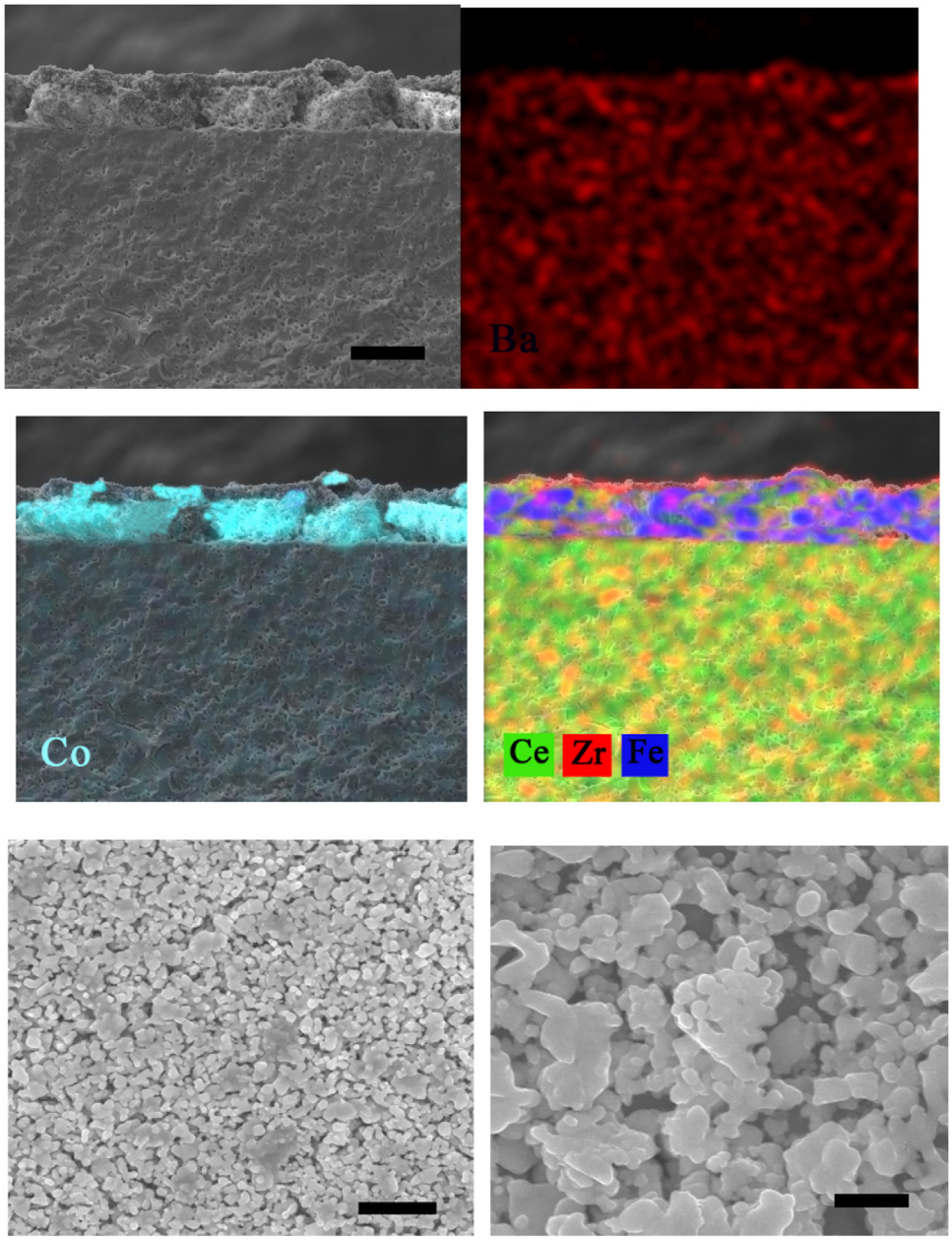

Fig. 3. SEM images of BSCF+BCZY/BCZY pellet cross-section a), Co mapping b), Ba mapping c) and Ce Cr and Fe mapping d), top view e) and f), the bar in a) b) and c) is 10, 5, 1 μm, respectively.

3. Results and discussion

3.1. Characterization

All XRD patterns of the compositions after sintering are presented in Fig. 1. The positions of the XRD peaks (100), (110), (111), (200), (210), (211),(220) and (310) of pure BSCF phase were preserved. Also, the positions of the XRD peaks (110), (111), (200), (211), (220) and (310) of pure BCZY phase were preserved. The XRD retrieved from the surface of the electrode of BSCF + BCZY is a combination of both phases, assigned to two single perovskite structure, suggesting that the BSCF and BCZY do not react in air up to 1000 °C. The TGA/DSC analysis of the BSCF + BCZY composite have been performed confirm the thermal stability during the heating process, Fig. 2. As we can see from the profiles of TGA/DSC, only 1.2% weight loss was observed from room temperature to 1000 °C which was attributed to the oxygen vacancy generation due to losing oxygen from the lattices of BSCF and BCZY during heat treatment. The combined TGA/DSC and XRD results of Figs. 1 and 2, respectively, confirm that the BSCF + BCZY can be easily synthesized by the solid state method and offers stability in air up to 1000 °C.

3.2. FE-SEM analysis on the microstructure

The evaluation of the microstructure, mainly the thickness of the film, particle size and the porosity was performed by SEM. Representative SEM images of BSCF + BCZY/BCZY pellet, with corresponding EDS elemental mapping are presented in Fig. 3. The cross-sectional view of a fractured surface of the prepared cell showed the deposited electrode film with ~10 μm thickness was well bonded with the electrolyte. The cell is electrolyte supported and the total thickness is around 1 mm, Fig. 3a). Ba mapping suggested that the BSCF and BCZY formed a continuous interconnected network inside the electrode since it was not possible to distinguish

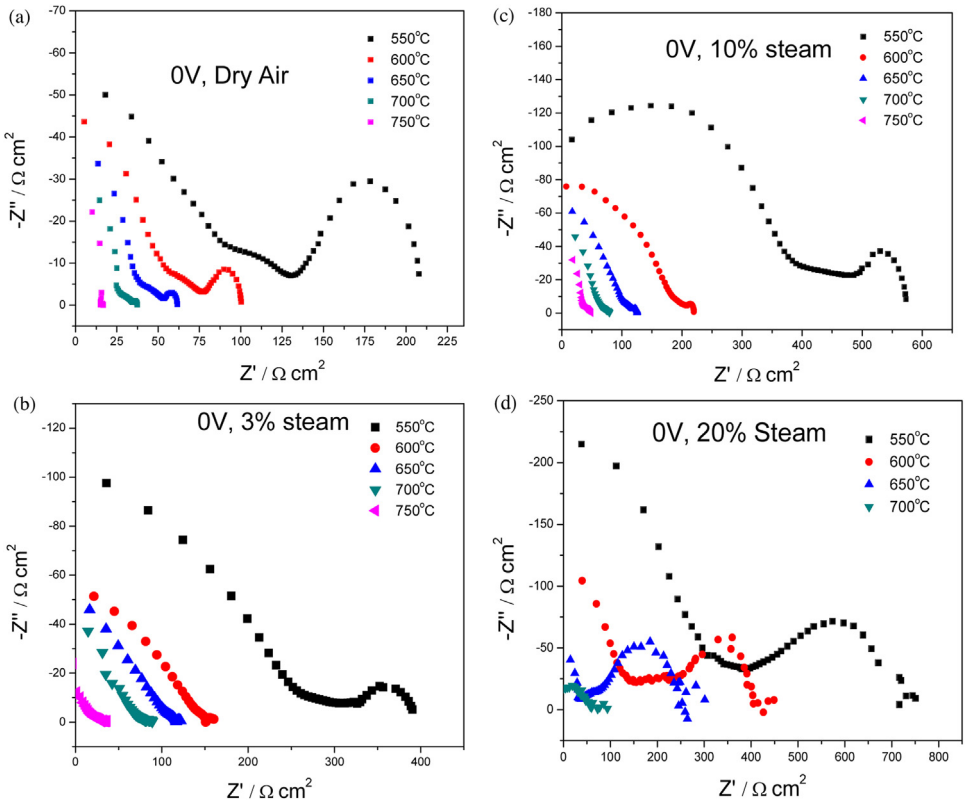

Fig. 4. pH_2O dependent analysis at different temperatures under OCV conditions.

from the two phases, Fig. 3b). Co mapping however, confirmed the chemical stability between BSCF and BCZY, where the clear interface can be observed. Fe, Zr and Ce mapping further proved this, Fig. 3c) and Fig. 3d). Fig. 3e) and f) are the surface analysis of the electrode, as could be seen the particle size was around 500 nm to 1 μm. The porosity was calculated to be 28%, resulting from the modest interconnectivity of the grains with the addition of open space which is ideal for the water steam diffusion. As pointed by Kröger-Vink reaction $H_2O + V_O^{\cdot\cdot} + O_O^{\times} \rightarrow 2(OH)_O^{\cdot}$, the dissociative absorption of water is the leading reaction that causes the formation of protonic defects in BCZY at high temperatures, in the presence of oxide ion vacancies. The following steps describe how protonic defects are formed: water vapor is divided into proton and a hydroxide ion, which incorporates into an oxide ion vacancy. Meanwhile, a covalent bond is generated by the proton to combine with oxygen in lattice. The water adsorption is an exothermic reaction and this is the reason why protons play a dominant role in conduction mechanism and oxygen vacancies at both low temperature and high temperature. Protons present as defects in equilibrium in the ambient of water vapor. Due to the negative enthalpy and entropy of hydration, higher temperatures lead to a reversible loss of protons. The concentration of protonic defects is not only regarded as a function of temperature, but also changes with water partial pressure. In order to get a better understanding of the composite electrode and a better understanding of the electrochemical catalytic mechanism, pH_2O dependent analysis at different temperatures is performed.

3.3. pH_2O dependent analysis at different temperatures

Fig. 4 is the pH_2O dependent analysis at different temperatures under OCV conditions. It can be seen that with the increase of temperature, the area specific resistance (ASR) of the electrode decreases dramatically, showing that the temperature is the dominant parameter for the electrocatalytic activity. In Fig. 4(a), under OCV condition, the ASR drops 20 times, from 550 to 750 °C; When the temperature is the same, the ASR increases with the water partial pressure. For example, at 600 °C, as profiled by the red line, the ASR increases from 100 to 400 Ωcm^2.

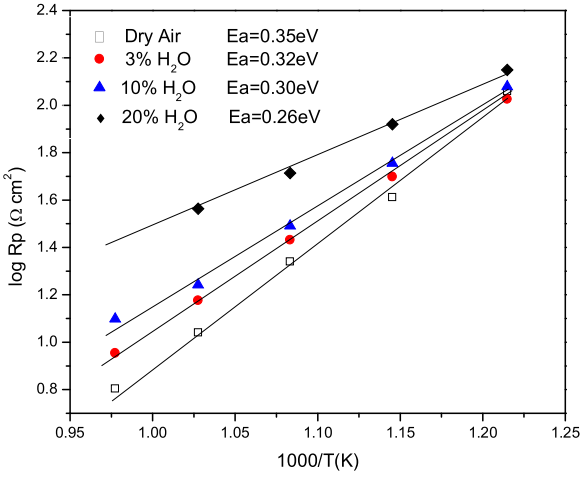

Fig. 5. Arrhenius plot under different water partial pressure.

The proton concentration increases with water partial pressure, which reaches a value in consistent with saturation limit. This explained the tendency of higher pH2O, higher R. Fig. 5 is the Arrhenius plot under different water partial pressure from 550 to 750 °C. We can see the activation energy for the composite electrode drops from 0.35 eV under dry condition to 0.26 eV with 20% vol water content. Different research groups have classified the proton transport mechanism with slight distinction on the rules. For the vehicle mechanism, protons diffuse with a "vehi-

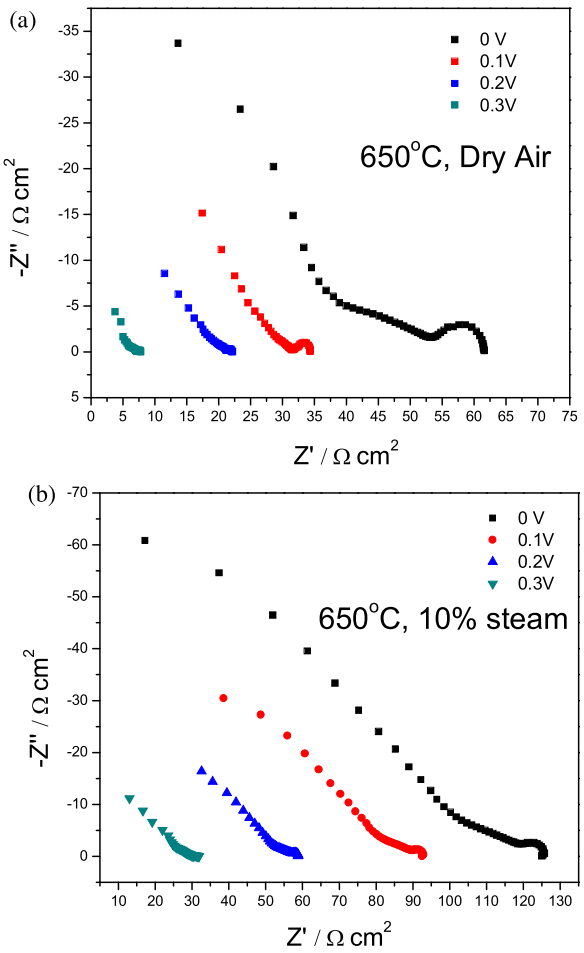

Fig. 6. Polarization analysis at 650 °C under dry and 10% steam conditions.

cle" such as H_3O^+ and commonly encounter in aqueous solution and other polymer membranes. Grotthuss mechanism, in opposition to the vehicle mechanism, believes that protons diffuse rotationally through a combination of molecular reorientation and they jump to a neighboring one from one oxygen ion. A recent analysis of quantum molecular dynamics (MD) simulation indicated that proton transfer reaction and proton rotational diffusion are very likely to be a rate-determining process, which could solve the contradictions of different experimental and computational data [15–19].

We can see from Fig. 6, at the same temperature, no matter in dry or wet conditions, with polarization imposed on the electrodes, the ASR decreases greatly. The tendency of lowering ASR is more obvious in dry conditions, 7 times comparing to that of 4 times with 10% steam.

4. Conclusions

In this work, $Ba_{0.5}Sr_{0.5}Co_{0.8}Fe_{0.2}O_{3-\delta}$-$BaCe_{0.4}Zr_{0.4}Y_{0.2}O_{3-\delta}$ composite electrode was successfully fabricated and the two phases are chemically compatible up to 1000 °C. The polarization behavior of BSCF-BCZY electrode under steam electrolysis conditions was studied. The electrode ASR became smaller with the increase of the bias polarization under the same water vapor partial pressures. The total resistance of the electrode was shown to be significantly affected by temperature, with the same level of pH_2O and bias polarization voltage. This result highlights BSCF-BCZY as an effective oxygen electrode under moderate polarization and pH_2O conditions, providing a new route for potential electrode of PCECs.

Acknowledgment

The authors acknowledge the Portuguese Foundation for Science and Technology (FCT) for financial support via the SFRH/BPD/86336/2012 and POPH, FCT Investigator Programme, project IF/00280/2012, Portugal and the European Social Fund, European Union. Additional financial supports also come from, QREN, FEDER, COMPETE for the Organic Chemistry Research Unit (QOPNA) (PEst-C/QUI/UI0062/2013; FCOMP-01-0124-FEDER-037296), National Natural Science Foundation of China (21377008, 21477005, U1507108), National High Technology Research and Development Program of China (2015AA034603), Beijing Nova Program (Z141109001814106), and Natural Science Foundation of Beijing Municipal Commission of Education (KM201410005008).

References

[1] I.P. Jain, C. Lal, A. Jain, Int. J. Hydrogen Energy 10 (2010) 5133.
[2] C.J. Winter, Int. J. Hydrogen Energy (Suppl. 14) (2009) S1.
[3] M.R. Ball, M. Wietschel, Int. J. Hydrogen Energy 2 (2009) 615.
[4] I.P. Jain, Int. J. Hydrogen Energy 17 (2009) 7368.
[5] B.C.H. Steele, A. Heinzel, Nature 414 (2001) 345.
[6] A. Boudghene Stambouli, E. Traversa, Renewable Sustainable Energy Rev. 6 (2002) 297.
[7] N. Zakowsky, S. Williamson, J.T.S. Irvine, Solid State Ionics 176 (2005) 3019.
[8] K.D. Kreuer, Annu. Rev. Mater. Res. 33 (2003) 333.
[9] N. Maffei, L. Pelletier, J.P. Charland, A. McFarlan, Fuel Cells 7 (2007) 323.
[10] Y. Yamazaki, P. Babilo, S.M. Haile, Chem. Mater. 20 (2008) 6352.
[11] I. Antunes, A. Brandao, F.M. Figueiredo, J.R. Frade, J. Gracio, D.P. Fagg, J. Solid State Chem. 182 (2009) 2149.
[12] T. Yang, F. Loureiroa, R. Queirósb, D. Pukazhselvan, I. Antunesc, J.A. Saraiva, Int. J. Hydrogen Energy 41 (2016) 11510.
[13] N. Narender, J.A. D.PAN, D. Saraiva, Int J Fagg, Hydrogen Energy 38 (2013) 8461.
[14] S.R. Jain, K.C. Adiga, V.R. Pai Verneker, Flame 40 (1981) 71.
[15] S. Pylaeva, C. Allolio, B. Koeppe, G.S. Denisov, H.H. Limbach, D. Sebastiani, P.M. Tolstoy, Phys. Chem. Chem. Phys. 17 (2015) 4634.
[16] M. Lindgren, A. Laaksonenb, P.O. Westlund, Phys. Chem. Chem. Phys. 11 (2009) 10368.
[17] M. Gutman, E. Nachliel, R. Friedman, Biochim. Biophys. Acta 1757 (2006) 931.
[18] R.I. Cukier, Biochim. Biophys. Acta 1656 (2004) 189.
[19] B. Merinova, W. Goddard III, J. Chem. Phys. 130 (2009) 194707.